Global Journal of Science Frontier Research: F
Mathematics and Decision Sciences
Volume 16 Issue 3 Version 1.0 Year 2016
Type : Double Blind Peer Reviewed International Research Journal
Publisher: Global Journals Inc. (USA)
Online ISSN: 2249-4626 & Print ISSN: 0975-5896

Effects of Nonisothermality and Wind-Shears on the Propagation of Gravity Waves (I): Comparison between *Hines*' Model and WKB Approach

By J. Z. G. Ma
California Institute of Integral Studies, United States

Abstract- In the presence of the vertical temperature & wind-speed gradients, we extend *Hines*' isothermal and shear-free model to calculate the vertical wavenumber (m_r) and growth rate (m_i) of gravity waves propagating in a stratified, non-isothermal, and wind-shear atmosphere. The profiles obtained from the extended Hines' model are compared with those from the Wentzel-Kramers-Brillouin (WKB) approach up to 300 km altitude. The empirical neutral atmospheric and wind models (NRLMSISE-00 and HWM93) are used to obtain the vertical profiles of the mean-field properties and the zonal/meridional winds.

GJSFR-F Classification : *MSC 2010: 76B15*

Strictly as per the compliance and regulations of :

Notes

Effects of Nonisothermality and Wind-Shears on the Propagation of Gravity Waves (I): Comparison between *Hines*' Model and WKB Approach

J. Z. G. Ma

Abstract- In the presence of the vertical temperature & wind-speed gradients, we extend *Hines'* isothermal and shear-free model to calculate the vertical wavenumber (m_r) and growth rate (m_i) of gravity waves propagating in a stratified, non-isothermal, and wind-shear atmosphere. The profiles obtained from the extended *Hines'* model are compared with those from the Wentzel-Kramers-Brillouin (WKB) approach up to 300 km altitude. The empirical neutral atmospheric and wind models (NRLMSISE-00 and HWM93) are used to obtain the vertical profiles of the mean-field properties and the zonal/meridional winds. Results show that (1) relative to the WKB model, extended *Hines'* m_i -profile deviates further away from *Hines'* model due to the lack of the non-isothermal effect; (2) the m_r-profiles obtained from both the extended *Hines'* and WKB models superimpose upon each other, and amplify *Hines'* m_r- magnitude; (3) the extended *Hines'* model provides identical perturbations for all physical quantities (i.e., pressure, density, temperature, wind components) which diverge the most from *Hines'* model in the 100-150 km layer; while the WKB model presents respective growths for different parameters, however, with the same vertical wavelengths which is not constant; and, (4) with the increase of phase speed (C_{ph}), while Hines' m_i - profile kee ps constant, the m_i-profiles of the extended Hines' and WKB models drop down and soars up, respectively; by contrast, the m_r-profiles of the three models fall off monotonously when C_{ph}/C (where C is sound speed) is no more than 0.75, but the profiles of the extended *Hines'* and WKB models overlap upon each other below 0.6, which shift away from *Hines'* model.

I. Introduction

Atmospheric thermal structure and background winds substantially influence the propagation of gravity waves in regions where thermal and/or Doppler ducting is confirmed either theoretically (e.g., *Pitteway & Hines* 1965; *Wang & Tuan*, 1988; Hickey 2001; *Walterscheid et al.* 2001; *Snively & Pasko* 2003; *Yu & Hickey* 2007a,b,c) or experimentally (e.g., *Hines & Tarasick* 1994; *Taylor et al.* 1995; *Isler et al.* 1997; *Walterscheid et al.* 1999; *Hecht et al.* 2001; *Liu & Swenson* 2003; *She et al.* 2004; *Snively et al.* 2007; *She et al.* 2009). The vertical variations in temperature and zonal/medidional wind shears have therefore become the two dominant factors and received increasing attentions in the transport, reflection, refraction, dissipation, and evanescence of gravity waves propagating in atmosphere. Accordingly, *Hines* (1960)'s locally isothermal, shear-free gravity wave theory with the WKB approximation has been extended by previous authors to ob-

Author: California Institute of Integral Studies, San Francisco, CA, USA. e-mail: zma@mymail.ciis.edu

tain generalized dispersion relations for accommodating to more complicated atmospheric situations.

Einaudi & *Hines* (1971) formulated an anelastic dispersion relation that includes the thermal and homogeneous wind effects, nevertheless in the absence of vertical wind shears, with the same growth rate (m_i) but an updated vertical wave number square (m_r^2) from *Hines'* formula ($m_{r\text{Hines}}^2$), expressed by

$$m_i = -\frac{1}{2H} \; ; \quad m_{r\text{Hines}}^2 = \frac{\Omega^2 - \omega_a^2}{C^2} + k_h^2 \frac{\omega_b^2 - \Omega^2}{\Omega^2} \quad \Rightarrow \quad m_r^2 = \frac{\Omega^2 - \omega_a^2}{C^2} + k_h^2 \frac{\omega_B^2 - \Omega^2}{\Omega^2} \quad (1)$$

where $\Omega = \omega - \mathbf{k}_h \cdot \mathbf{v}_0$ is the intrinsic (or, Doppler-shifted) angular frequency, ω is the extrinsic (ground-based) frequency, $\mathbf{k}_h$ is the horizontal wavenumber vector, $\mathbf{v}_0$ is the horizontal mean-field wind vector, $C = \sqrt{\gamma g H}$ is the sound speed in which γ is the adiabatic index, g is the gravitational acceleration, and, H is Hines' scale-height, ω_B is the non-isothermal Brunt-Väisälä buoyancy frequency, and ω_a is the isothermal acoustic-cutoff frequency. The thermal effect is given in the definition of ω_B with $\omega_B^2 = \omega_b^2 + g k_T$ [in which $\omega_b^2 = (1-1/\gamma)(g/H)$ is Hines' isothermal buoyancy frequency, and $k_T = (\mathrm{d}H/\mathrm{d}z)/H$ is the thermal inhomogeneous number], and the wind effect is implicitly involved in Ω. Note that Eq.(1) is an extended *Hines* (1960)' expression which recovers his original windless result for $k_T = 0$ and $\mathbf{v}_0 = 0$. The last $\Omega - m_r$ dispersion equation in Eq.(1) is widely used in gravity wave studies as *Hines'* locally isothermal and shear-free model.

Later, *Gossard* & *Hooke* (1975) introduced the structure and behavior of the highest-frequency gravity waves in the mesosphere. The result was the same as Eq.(1) but without the first term. By considering the Coriolis parameter (*Eckart* 1960), Marks & Eckermann (1995) and *Eckermann* (1997) updated Eq.(1) to expose the effect of the Earth's rotation effect, as well as wave refraction, saturation, and turbulent damping via ray-tracing mapping. *Vadas* & *Fritts* (2004,2005) adopted Hines' isothermal model to examine the influence of dissipation terms, like kinematic viscosity and thermal diffusivity, and derived a complex dispersion relation and GW damping rate arising from mesoscale convective complexes in the thermosphere. Note that in the last formula of Eq.(1), the thermal effect is present in ω_B, but missing in ω_a. Besides, these studies did not take into consideration the wind-shear effect (i.e., $\omega_{\mathrm{v}} = |\mathrm{d}\mathbf{v}_0/\mathrm{d}z|$), but assuming a uniform background horizontal wind.

The role played by shears in gravity wave propagation was dominantly recognized at first through discussions of linear instabilities in a 2D, stably-stratified, horizontal shear flows of an ideal Boussinesq fluid (*Miles* 1961; *Howard* 1961), as well as of the onset of atmospheric turbulence (e.g., *Hines* 1971; *Dutton* 1986). It was found that the isothermal (gradient) Richardson number, $Ri = \omega_b^2/\omega_{\mathrm{v}}^2$, has a critical value, $Ri_c = 1/4$. If $Ri > Ri_c$, flows are stable everywhere; however, this criterion may not rigorously apply for all scenarios, but as a necessary, not sufficient condition for instabilities (*Stone* 1966; *Miles* 1986), particularly when, e.g., the shear is tilted from zenith (*Sonmor* & *Klaassen* 1997), or, when the molecular viscosity is important (*Liu* 2007). Even for all arbitrarily large values of Ri, a family of explicit, elementary, stably-stratified, time-dependent, and non-parallel

Notes

flows was verified to be unstable (*Majda* & *Shefter* 1998). A growing body of experimental and observational data also indicated that turbulence survives $Ri \gg 1$ (*Galperin et al.* 2007). Notwithstanding the above, there has been no such a dispersion relation of gravity waves which is derived to get Ri and Ri_c directly by solving the linear fluid equations under the WKB approximation.

Notes

Fortunately, sheared atmosphere had already been studied for tens of years before *Hines* (1960)'s WKB work. A special treatment was adopted to the perturbation of fluid equations in an incompressible atmosphere ($\gamma \to \infty$): linear wavelike solutions are assumed in time and horizontal coordinates, with ω, k_h, and the mean-field state varying neither in time nor in the horizontal plane. As such the perturbed vertical profiles of bulk properties are obtained in view of the vertical variation in the background temperature and horizontal velocity (*Taylor* 1931; *Goldstein* 1931; see a review by *Fritts* & *Alexander* 2003). This approach has now been developed fully numerically as a generalized full-wave model (FWM) to treat the propagation of non-hydrostatic, linear gravity waves in a realistic compressible, inhomogeneous atmosphere which is dissipative due to not only the eddy processes in the lower atmosphere but also the molecular processes (viscosity, thermal conduction and ion drag) in atmosphere, in addition to the altitude-dependent mean-field temperature and horizontal winds, as well as Coriolis force (Hickey 2011; Hickey et al. 1997,1998,2000,2001,2009,2010; *Walterscheid* & *Hickey* 2001,2005,2012; *Schubert et al.* 2003,2005). Importantly, the WKB approach has been employed to yield a Taylor-Goldstein equation or a more generalized quadratic equation and the non-isothermal and shearing effects can be obtained in the presence of the height-varying temperature and wind shears (see, e.g., *Beer* 1974; Nappo 2002; *Sutherland* 2010). The most recent contribution was performed by *Zhou* & *Morton* (2007). Upon the background gradient properties of the atmosphere, the authors found that the vertical wavenumber depends only on the intrinsic horizontal phase speed ($C_{ph} = \Omega/k_h$). Unfortunately, the generalized dispersion equation is unable to restore Eq.(1) due to some algebra inconsistencies.

we are inspired to concentrate on the exact expressions of the dispersion relation obtained by extending *Hines'* model and by adopting the WKB approximation. The purpose lies in describing the features of gravity wave propagation in a compressible and non-isothermal atmosphere in the presence of atmospheric wind shears. The motivation to tackle this subject is the necessity to find an accurate gravity wave model in data-fit modeling to demonstrate the modulation of waves excited by natural hazards (like, tsunami/vocano events, nuclear explosion, etc.) in realistic atmosphere. The region concerned is from the sea level to ∼200 km altitude within which the atmosphere is non-dissipative (negligible viscosity and heat conductivity) and the ion drag and Coriolis force can be reasonably omitted (*Harris* & *Priester* 1962; *Pitteway* & *Hines* 1963; *Volland* 1969a,b). The structure of the paper is as follows: Section 2 extends *Hines'* model, Eq.(1), by involving the nonthermaility and wind-shears in the dispersion relation. Section 3 gives a generalized dispersion relation by employing the WKB approach. Section 4 compares the two models and illustrates their deviations from *Hines'* isothermal and shear-free model. Section 5 offers a summary and conclusion. In the study, the mean-field properties up to 300 km

altitude are obtained from the empirical neutral atmospheric model (NRLMSISE-00; *Picone et al.* 2002) and the horizontal wind model (HWM93; *Hedin et al.* 1996). We choose a Cartesian frame, $\{\hat{\mathbf{e}}_x, \hat{\mathbf{e}}_y, \hat{\mathbf{e}}_z\}$, where $\hat{\mathbf{e}}_x$ is horizontally due east, $\hat{\mathbf{e}}_y$ due north, and $\hat{\mathbf{e}}_z$ vertically upward.

II. Extended Hines' Model: Dispersion Relation

Up to ∼200 km altitude, the neutral atmosphere can be considered non-dissipative with negligible eddy process, molecular viscosity and thermal conduction, ion-drag, and Coriolis effect (*Harris & Priester* 1962; *Pitteway & Hines* 1963; *Volland* 1969a,b). The governing non-hydrostatic and compressible equations to describe gravity waves are based on conservation laws in mass, momentum, and energy, as well as the equation of state (e.g., *Beer* 1974; *Fritts & Alexander* 2003; *Zhou & Morton* 2007; for a complete set of equations including dissipative terms, see, e.g., *Landau & Lifshitz* 1959; *Volland* 1969a; *Francis* 1973; *Hickey & Cole* 1987; *Vadas & Fritts* 2005; *Liu et al.* 2013):

$$\frac{D\rho}{Dt} = -\rho\nabla\cdot\mathbf{v}, \quad \frac{D\mathbf{v}}{Dt} = -\frac{1}{\rho}\nabla p + \mathbf{g}, \quad \frac{Dp}{Dt} = -\gamma p\nabla\cdot\mathbf{v}, \quad p = \rho R_s T \tag{2}$$

in which $\mathbf{v}$, ρ, p, and T are the atmospheric velocity, density, pressure, and temperature, respectively; $D/Dt = \partial/\partial t + \mathbf{v}\cdot\nabla$ is the substantial derivative over time t; $\mathbf{g} = \{0, 0, -g\}$ is the gravitational acceleration; and γ and R_s are the adiabatic index and gas constant, respectively. The vertical profiles of Hines' scale height H, and these three input parameters, γ, g, and R_s, are given in Fig.1, where two additional scale heights, H_ρ (in density) and H_p (in pressure), are also shown for comparisons with H, the definitions of which are given below in Eq.(4).

Acoustic-gravity waves originate from the small perturbations away from their mean-field properties and propagate in a stratified atmosphere (*Gossard & Hooke* 1975). We linearize Eq.(2) by employing

$$\left.\begin{array}{l} \rho = \rho_0 + \rho_1, T = T_0 + T_1, p = p_0 + p_1 \\ \mathbf{v} = \mathbf{v}_0 + \mathbf{v}_1 = \{U, V, 0\} + \{u, v, w\} \\ \left(\frac{\rho_1}{\rho_0}, \frac{p_1}{p_0}, \frac{T_1}{T_0}, \frac{u}{U}, \frac{v}{V}, w\right) \propto e^{i(\mathbf{k}\cdot\mathbf{r}-\omega t)} \end{array}\right\} \tag{3}$$

where parameters attached by subscript "$_0$" are ambient mean-field components and those with subscript "$_1$" are the linearized quantities; U and V are the zonal (eastward) and meridional (northward) components of the mean-field wind velocity (note that the wind is horizontal and thus the vertical component W is zero), respectively; (u, v, w) are the three components of the perturbed velocity, respectively; $\mathbf{k} = \{k, l, m\}$ in which k and l are the two horizontal wavenumbers which are constants, constituting a horizontal wave vector $\mathbf{k}_h = \{k, l\} = k_h\mathbf{k}_{h0}$ with $k_h = \sqrt{k^2 + l^2}$ and $\mathbf{k}_{h0} = \mathbf{k}_h/k_h$, and, $m = m_r + im_i$ is the vertical wave vector which is a complex; and, ω is the extrinsic angular wave frequency which is a constant. The inhomogeneities of the mean-field properties bring about following altitude-dependent parameters:

$$k_\rho = \frac{1}{H_\rho} = \frac{\mathrm{d}(\ln\rho_0)}{\mathrm{d}z},\ k_p = \frac{1}{H_p} = \frac{\mathrm{d}(\ln p_0)}{\mathrm{d}z},\ k_T = \frac{\mathrm{d}(\ln T_0)}{\mathrm{d}z},\ \omega_\mathrm{v} = \sqrt{\left(\frac{\mathrm{d}U}{\mathrm{d}z}\right)^2 + \left(\frac{\mathrm{d}V}{\mathrm{d}z}\right)^2} \quad (4)$$

in which k_ρ, k_p, and k_T are the density, pressure, and temperature scale numbers, respectively, satisfying $k_T = k_p - k_\rho$ from the equation of state. Note that ω_v is the shear-related parameter in the unit of angular frequency, rad/s.

Notes

The linearization of Eq.(2) yields following set of perturbed equations:

$$\left.\begin{array}{l} \frac{\partial\rho_1}{\partial t} + \mathbf{v}_0\cdot\nabla\rho_1 + \mathbf{v}_1\cdot\nabla\rho_0 + \rho_0\nabla\cdot\mathbf{v}_1 + \rho_1\nabla\cdot\mathbf{v}_0 = 0 \\ \frac{\partial\mathbf{v}_1}{\partial t} + \mathbf{v}_1\cdot\nabla\mathbf{v}_0 + \mathbf{v}_0\cdot\nabla\mathbf{v}_1 = -\frac{1}{\rho_0}\nabla p_1 + \frac{\rho_1}{\rho_0}\mathbf{g} \\ \frac{\partial p_1}{\partial t} + \mathbf{v}_0\cdot\nabla p_1 + \mathbf{v}_1\cdot\nabla p_0 = -\gamma p_0\nabla\cdot\mathbf{v}_1 - \gamma p_1\nabla\cdot\mathbf{v}_0 \\ \frac{p_1}{p_0} = \frac{\rho_1}{\rho_0} + \frac{T_1}{T_0} \end{array}\right\} \quad (5)$$

which provides following dispersion equation:

$$\begin{bmatrix} \omega & k & l & m - ik_\rho & 0 \\ 0 & \omega & 0 & i\frac{\mathrm{d}U}{\mathrm{d}z} & k \\ 0 & 0 & \omega & i\frac{\mathrm{d}V}{\mathrm{d}z} & l \\ -ig & 0 & 0 & \omega & m - ik_p \\ 0 & k & l & m - i\frac{k_p}{\gamma} & \frac{\omega}{C^2} \end{bmatrix} \begin{bmatrix} \frac{\rho_1}{\rho_0} \\ u \\ v \\ w \\ \frac{p_1}{p_0} \end{bmatrix} = 0 \quad (6)$$

from which a generalized, complex dispersion relation of gravity waves is derived in the presence of non-isothermality and wind shears, if and only if the determinant of the coefficient matrix is zero:

$$\Omega^4 - \left(C^2K^2 + gk_T\right)\Omega^2 - (\gamma-1)gk_h\Omega V_{k1} + C^2k_h^2\omega_B^2 = i\gamma gm\Omega\left(\Omega - k_hHV_{k1}\right) \quad (7)$$

in which $\Omega = \omega - \mathbf{k}_h\cdot\mathbf{v}_0 = \omega - (kU + lV) = \omega - k_hV_k$ is the intrinsic (or, Doppler-shifted) angular frequency, $K^2 = k_h^2 + m^2$, $V_k = \mathbf{k}_{h0}\cdot\mathbf{v}_0 = \sqrt{U^2+V^2}\cos\theta$, and $V_{k1} = \mathbf{k}_{h0}\cdot(d\mathbf{v}_0/dz) = \omega_\mathrm{v}\cos\theta'$, where θ and θ' are the angles between the horizontal wave vector $\mathbf{k}_h$ and (1) the mean-field wind velocity $\mathbf{v}_0$, (2) the wind velocity gradient, respectively. Note that $\theta = \theta'$ if θ' is independent of z.

Because m is a complex, using $(m_r + im_i)$ instead of m in Eq.(7) produces the solutions of the dispersion relation:

$$m_i = \left(-\frac{1}{2} \quad \frac{1}{H} - \frac{V_{k1}}{C_{ph}}\right) \quad (8)$$

and

$$\Omega^4 - \left[C^2 \quad k_h^2 + m_r^2 - \frac{2-\gamma}{2\gamma}\frac{1}{H}\frac{V_{k1}}{C_{ph}}\right) + \omega_A^2\Big]\Omega^2 + C^2 k_h^2 \omega_B^2 \left(1 - \frac{\cos^2\theta'}{4R_I}\right) = 0 \qquad (9)$$

which can be expressed alternatively as follows:

$$m_r^2 = \frac{\Omega^2 - \omega_A^2}{C^2} + k_h^2 \frac{\omega_B^2 - \Omega^2}{\Omega^2} + \frac{1}{2}\frac{V_{k1}}{C_{ph}}\left(\frac{2-\gamma}{\gamma H} - \frac{1}{2}\frac{V_{k1}}{C_{ph}}\right) \qquad (10)$$

in which $C_{ph} = \Omega/k_h$ is the intrinsic horizontal phase speed, $\omega_A^2 = \omega_a^2 + gk_T$ is the nonisothermal acoustic-cutoff frequency, and $R_I = R_i + gk_T/\omega_{\rm v}^2$ is the nonisothermal (gradient) Richardson number.

The last equation in Eq.(3) reveals that the amplitude (denoted by A^* as follows) of all the perturbations grows exponentially by following the same growth:

$$A^* \propto e^{-m_i z} \text{ for } m_i \text{ independent of } z; A^* \propto e^{-\int m_i \mathrm{d}z} \text{ for } m_i \text{ dependent of } z \qquad (11)$$

Under shear-free conditions ($V_{k1} = 0$), Eq.(11) recovers the growth, $A(0)e^{z/2H}$, of Hines' classical result. Note that the temperature gradient, as represented by k_T, does not influence the amplitude growth; and, only in the presence of the shear can the horizontal phase speed (C_{ph}) come into play to modulate the growth.

Eq.(9) is a quadratic equation of Ω^2. It is easy to see that for small shear ($V_{k1}/HC_{ph} \ll m_r^2$) there exists a critical value of $R_{Ic} = \cos^2\theta'/4$. Note that the inclusion of θ' is consistent with the result shown in Hines (1971). If $R_I < R_{Ic}$, one solution of Ω^2 is negative and thus turbulence can be completely excluded; otherwise, if $R_I > R_{Ic}$, the two roots of Ω^2 are always positive and any turbulence is suppressed. Under isothermal condition, this nonisothermal result recovers the conclusion introduced by *Hines* (1971) and *Dutton* (1986) with $\theta' = 0$. However, if the shear is large enough, the coefficient of Ω^2 in Eq.(9) may be positive. On the one hand in this case, $R_I > R_{Ic}$ always leads to negative Ω^2 and turbulence is inevitably excited; on the other hand, $R_I < R_{Ic}$ gives one negative root of Ω^2, meaning turbulence can be developed. As a result, from our WKB dispersion relation, we confirm that the criterion of $R_{Ic} = 1/4$ is merely as a necessary but not sufficient condition for instabilities (*Stone* 1966; *Miles* 1986).

Eq.(10) makes us easier to identify the effects of nonisothermality and wind shear on the propagation of gravity waves by comparison with previous dispersion relations introduced in literature. First of all, by assuming $k_T = 0$ and $\mathbf{v}_0 = 0$, Hines (1960)'s dispersion relation for an isothermal and windless atmosphere is recovered, with $\omega_A \to \omega_a$, $\omega_B \to \omega_b$, and $V_{k1} \to 0$. Secondly, for a nonisothermal and windless atmosphere, *Einaudi* & *Hines* (1971)'s result as shown in Eq.(1) is produced, certainly after the correction of the erroneous isothermal cutoff frequency ω_a replaced by the nonisothermal ω_A. We stress here that, although Eq.(1) is widely used as the dispersion relation for nonisothermal atmosphere by almost all the previous authors in both theoretical modeling and data

analysis, the formula is not accurate because it has a wrong expression of the cutoff frequency, which leads to absurd result that buoyancy frequency can be larger than the cutoff frequency. We point out the buoyancy frequency can never be larger than the cutoff frequency for either an isothermal or nonisothermal case, and the accurate nonisothermal dispersion relation in an windless atmosphere is not Eq.(1), but as follows:

$$m_r^2 = \frac{\Omega^2 - \omega_A^2}{C^2} + k_h^2 \frac{\omega_B^2 - \Omega^2}{\Omega^2} \tag{12}$$

Lastly, Eq.(10) exposes that wind shear (V_{k1}) influences the vertical wave propagation always in combination with the intrinsic phase speed (C_{ph}), the same feature as that affecting the vertical amplitude growth rate in Eq.(8). Due to the fact that the inclusion of wind shear term in the dispersion relation of gravity waves has not been found in literature, we thus make use of the FWM approach to validate the wind-shear effect, as to be given in the next section.

III. WKB Approach

In the WKB approach, linear wavelike solutions are assumed in time and horizontal coordinates, however, not in the vertical direction; by contrast, the mean-field properties are supposed to vary only in the vertical direction. As a result, we follow Eq.(3) to linearize Eq.(2) by adopting

$$\left(\frac{\rho_1}{\rho_0},\ \frac{p_1}{p_0},\ \frac{T_1}{T_0},\ \frac{u}{U},\ \frac{v}{V}, w\right) \propto A(z) e^{i(\mathbf{k}_h \cdot \mathbf{r} - \omega t)} \tag{13}$$

in which $A(z)$ represents respective amplitude of all the perturbations. The resultant set of linearized equations is as follows:

$$\left.\begin{array}{l} i\left(ku + lv\right) + \frac{\partial w}{\partial z} + k_\rho w = i\Omega \frac{\rho_1}{\rho_0},\ i\left(ku + lv\right) + \frac{\partial w}{\partial z} + \frac{k_p}{\gamma} w = i\frac{\Omega}{\gamma}\frac{p_1}{p_0},\ \frac{p_1}{p_0} = \frac{\rho_1}{\rho_0} + \frac{T_1}{T_0} \\ i\Omega u - \frac{\partial U}{\partial z} w = ik\frac{C^2}{\gamma}\frac{p_1}{p_0},\ i\Omega v - \frac{\partial V}{\partial z} w = il\frac{C^2}{\gamma}\frac{p_1}{p_0},\ i\Omega w = g\frac{\rho_1}{\rho_0} + \frac{C^2}{\gamma}\left[\frac{\partial}{\partial z}\left(\frac{p_1}{p_0}\right) + k_p \frac{p_1}{p_0}\right] \end{array}\right\} \tag{14}$$

in which the reduction of variables yields following two coupled equations between w and p_1/p_0:

$$\left.\begin{array}{l} \gamma\Omega\frac{\partial w}{\partial z} + \left(\gamma \mathbf{k}_h \cdot \frac{d\mathbf{v}_0}{dz} - \frac{\Omega}{H}\right) w - i\left(\Omega^2 - C^2 k_h^2\right)\frac{p_1}{p_0} = 0 \\ i\left[\gamma\left(\Omega^2 - g k_T\right) H - g\left(\gamma - 1\right)\right] w - C^2 \Omega H \frac{\partial}{\partial z}\left(\frac{p_1}{p_0}\right) + g\left(\gamma - 1\right)\Omega H \frac{p_1}{p_0} = 0 \end{array}\right\} \tag{15}$$

This set of equations corrects Eq.(4) of *Zhou & Morton* (2007; hereafter ZM07) by

(1) updating ZM07's term of $\mathbf{k}_h \cdot (d\mathbf{v}_0/dz)$ with $\gamma \mathbf{k}_h \cdot (d\mathbf{v}_0/dz)$;

(2) updating ZM07's term of $i\left(\Omega^2 - C^2 k_h^2\right)$ with $-i\left(\Omega^2 - C^2 k_h^2\right)$;

(3) updating ZM07's term of $(p_1/p_0)\Omega H g + C^2 \Omega H (1/p_0)\partial p_1/\partial z$ with $(p_1/p_0)\Omega H g(\gamma - 1) - C^2 \Omega H \partial(p_1/p_0)/\partial z$.

Eqs.(14,15) provide a full set of governing equations for gravity wave propagation:

$$\frac{\partial^2 w}{\partial z^2} + f(z)\frac{\partial w}{\partial z} + g(z)w = 0, \quad \text{or,} \quad \frac{\partial^2 \tilde{w}}{\partial z^2} + q^2(z)\tilde{w} = 0 \tag{16}$$

together with

$$\left.\begin{aligned}
i\Omega\tfrac{p_1}{p_0} &= -(\beta-1)\left[\gamma\tfrac{\partial w}{\partial z} + \left(\gamma\tfrac{V_{k1}}{\Omega} + \tfrac{k_p}{k_h}\right)k_h w\right]\\
i\Omega\tfrac{\rho_1}{\rho_0} &= -(\beta-1)\left[\tfrac{\partial w}{\partial z} + \left(\tfrac{V_{k1}}{\Omega} + \tfrac{k_\rho}{k_h} + \tfrac{\beta}{\beta-1}\tfrac{k_p-\gamma k_\rho}{\gamma k_h}\right)k_h w\right]\\
i\Omega\tfrac{T_1}{T_0} &= -(\beta-1)\left\{(\gamma-1)\tfrac{\partial w}{\partial z} + \left[(\gamma-1)\tfrac{V_{k1}}{\Omega} + \tfrac{k_T}{k_h} - \tfrac{\beta}{\beta-1}\tfrac{k_p-\gamma k_\rho}{\gamma k_h}\right]k_h w\right\}\\
iku &= -\beta\tfrac{k^2}{k_h^2}\tfrac{\partial w}{\partial z} + \left[\tfrac{k}{\Omega}\tfrac{\partial U}{\partial z} - \beta\tfrac{k^2}{k_h^2}\left(k_h\tfrac{V_{k1}}{\Omega} - \tfrac{1}{\gamma H}\right)\right]w\\
il\upsilon &= -\beta\tfrac{l^2}{k_h^2}\tfrac{\partial w}{\partial z} + \left[\tfrac{l}{\Omega}\tfrac{\partial V}{\partial z} - \beta\tfrac{l^2}{k_h^2}\left(k_h\tfrac{V_{k1}}{\Omega} - \tfrac{1}{\gamma H}\right)\right]w
\end{aligned}\right\} \tag{17}$$

In the above, following functions are defined:

$$\left.\begin{aligned}
f(z) &= -\tfrac{1}{H} - \tfrac{d\left(\ln C_d^2\right)}{dz} = -\tfrac{1}{H} + \beta k_T + 2(\beta-1)\tfrac{V_{k1}}{C_{ph}}\\
g(z) &= \tfrac{1}{C_d^2}\left(\tfrac{1}{\beta-1}\omega_b^2 - 2V_{k1}^2\right) - \tfrac{1}{\beta}k_h^2 + \tfrac{\beta^2}{\beta-1}\tfrac{k_T}{\gamma H} + \tfrac{1}{C_{ph}}\left\{V_{k2} - \left[1+\beta\left(k_T H - \tfrac{2}{\gamma}\right)\right]\tfrac{V_{k1}}{H}\right\}\\
q^2(z) &= g(z) - \tfrac{1}{4}f^2(z) - \tfrac{1}{2}\tfrac{df}{dz} =\\
&= \tfrac{\Omega^2-\Omega_A^2}{C^2} + k_h^2\tfrac{\Omega_B^2-\Omega^2}{\Omega^2} + \beta\tfrac{V_{k1}}{C_{ph}}\left[\tfrac{2-\gamma}{\gamma H} - (3\beta-2)k_T - 3(\beta-1)\tfrac{V_{k1}}{C_{ph}} + \tfrac{V_{k2}}{V_{k1}}\right]
\end{aligned}\right\} \tag{18}$$

and following notations are applied:

$$\left.\begin{aligned}
&\omega = c_{ph}k_h,\ C_{ph} = c_{ph} - V_k,\ C^2 = C_{ph}^2 + C_d^2,\ k_{kT} = \tfrac{1}{k_T}\tfrac{dk_T}{dz}\\
&\beta = \tfrac{C^2}{C_d^2},\ \alpha = \tfrac{\gamma}{2}\left\{1+\beta\left[1+\tfrac{k_T}{k_p}\left(1+\tfrac{k_{kT}}{k_T} - \tfrac{3}{2}\beta\right)\right]\right\}\\
&V_{k2} = \mathbf{k}_{h0}\cdot\tfrac{d^2\mathbf{v}_0}{dz^2} = \tfrac{k}{k_h}\tfrac{d^2U}{dz^2} + \tfrac{l}{k_h}\tfrac{d^2V}{dz^2}\\
&\omega_b^2 = \tfrac{\gamma-1}{\gamma}\tfrac{g}{H},\ \Omega_B^2 = \omega_B^2 + (\beta-1)gk_T;\ \omega_a^2 = \tfrac{C^2}{4H^2},\ \Omega_A^2 = \omega_A^2 + (\alpha-1)gk_T
\end{aligned}\right\} \tag{19}$$

where c_{ph} is the extrinsic horizontal phase speed; C_d is the complementary phase speed introduced for mathematical convenience; k_{kT} is the inhomogeneous number of k_T; α and β are altitude-dependent coefficients determined by atmospheric inhomogeneities irrelevant of wind shears; V_{k2} is another input parameter, in addition to V_{k1}, contributed by wind shears. Note that the two newly introduced pseudo-frequencies, Ω_A and Ω_B, are contributed by wave-independent frequencies, ω_A and ω_B, and wave-dependent components, $(\alpha-1)gk_T$ and $(\beta-1)gk_T$, respectively.

As ZM07 pointed out, Eq.(16) reduces to the traditional Taylor-Goldstein equation if there is no temperature variation and $\gamma \to \infty$ (e.g., *Nappo* 2002); the $q^2(z)$ recovers Hines (1960)' dispersion relation in a windless isothermal atmosphere; and, $w(z)$ yields Beer (1974)'s result under z-independent wind and non-isothermal conditions. However, we argue that ZM07's another claim, the signs of V_{k1}^2 [or, $(\mathbf{k}_h \cdot d\mathbf{v}_0/dz)^2$ in that paper] and k_T^2 [or, $(dH/dz)^2$ in that paper] in $q^2(z)$ are all negative which is "consistent with the fact

that gravity waves cannot propagate freely at discontinuous boundaries", is invalid due to the fact that the process is also determined by V_{k2}, while k_T^2 does not appear in $q^2(z)$ but k_{kT} occurs in α; more important, the buoyancy frequency ω_b and the cut-off frequency ω_a in ZM07's $q^2(z)$ must be replaced by ω_B and ω_A, respectively, due to the presence of k_T.

Notes

In the cumbersome Eq.(18), $q^2(z)$ could be either positive to describe freely upward/downward propagating waves in atmosphere, or negative to demonstrate evanescent "waves" (in fact "nonwaves" with infinite vertical wavelength) which are simply exponentially growing or decaying in amplitude. The choice of growing versus decaying is usually determined by things such as boundary conditions, or the finiteness of, e.g., energy. In its propagation, a wave can have $q^2(z) > 0$ at some altitudes in one region, and becomes evanescent with $q^2(z) < 0$ in a different region. At the boundary between two such regions where $q^2(z) = 0$, wave reflection and transmission occur. Interestingly, in the case of $q^2(z) > 0$, Eq.(18) provides the vertical wavenumber $m = m_r + im_i$ of the plane-wave solution with

$$m_i = \frac{1}{2}f(z) = -\frac{1}{2H} + \frac{\beta}{2}k_T + (\beta - 1)\frac{V_{k1}}{C_{ph}} \tag{20}$$

and

$$m_r^2 = q^2(z) \tag{21}$$

Notice that the above FWM solutions are not exactly the same as the WKB results given in Eq.(8) and Eq.(10), respectively, but with extra terms in addition to modifications.

IV. Comparison and Validation

a) Mean-field atmospheric properties

The unperturbed mean-field atmospheric properties and related gravity-wave parameters are calculated from two empirical, neutral atmospheric models: (1) NRLMSISE-00, developed by Mike Picone, Alan Hedin, and Doug Drob (*Picone et al.* 2002); and (2) the horizontal wind model, HWM93, developed by *Hedin et al.* (1996). We arbitrarily choose a position at 60° latitude and -70° longitude for a local apparent solar time of 1600 hour on the 172th day of a year, with daily solar $F_{10.7}$ flux index and its 81-day average of 150. The daily geomagnetic index is 4. Fig.2 demonstrates the results. The upper two panels illustrate the vertical profiles of mean-field mass density (ρ_0), pressure (p_0), temperature (T_0), sound speed (C), zonal (eastward) wind (U), and meridional (northward) wind (V), while the lower two ones present those of wave-relevant inhomogeneous scale numbers (k_ρ, k_p, and k_T), and atmospheric cut-off frequencies (ω_a under isothermal condition and ω_A under non-isothermal condition) as well as buoyancy frequencies (ω_b under isothermal condition and ω_B under non-isothermal condition).

The upper left panel gives ρ_0 (solid blue), p_0 (dash blue), C (solid red), and T_0 (dash red). The magnitude of ρ_0 decreases all the way up from 1.225 kg/m^3 (or, 2.55×10^{25} $1/m^3$) at the sea level to only 2.38×10^{-11} kg/m^3 (4.95×10^{14} /m^3) at 300 km altitude.

The value of p_0 has a similar tendency to ρ_0. It reduces from 10^5 Pa at the sea level to 8.27×10^{-6} Pa finally. T_0 is 281 °K at the sea level. It decreases linearly to 224 °K at 13 km, and then returns to 281 °K at 47 km, followed by a reduction again to 146 °K at 88 km. Above this height, the temperature goes up continuously and reaches a stable exospheric value of ∼1200 °K above 300 km height. At 194 km it is 1000 °K. Parameter C follows the variation of $T_0^{1/2}$. At the sea level, it is 336 m/s; at 300 km altitude, it is 697 m/s. The upper right panel exposes U (solid blue) and V (dash pink). Both of the horizontal wind components oscillate twice dramatically in altitude within ±51 m/s in amplitude below 200 km altitude, and above this height they grow roughly proportionally to the height.

In the lower left panel, three curves are illustrated: density scale number k_ρ (solid blue), pressure scale number k_p (dash red), and temperature scale number k_T (solid black). Clearly, up to 200 km altitude, $k_\rho \neq k_p$ always holds and thus the isothermal condition $k_T = 0$ is broken in atmosphere, except at three heights: 13.1 km, 47.2 km, and 87.9 km. However, above 100 km altitude, k_T eventually keeps its positive polarization after two times of adjustment from negative to positive values. Above 200 km altitude, $k_T = 0$ can be considered valid. Note that the scale height H is equal to $-1/k_p$. At the sea level, H is calculated as 8.44 km and then soaring to as high as 75.6 km when approaching to about 200 km altitude and beyond.

The lower right panel draws two pairs of frequencies of gravity waves: ω_A (solid red) & ω_a (dash red), and ω_B (solid blue) & ω_b (dash blue). At all altitudes, ω_a and ω_A are always larger than ω_b and ω_B, respectively. That is, $\omega_a > \omega_b$ and $\omega_A > \omega_B$ are guaranteed for all altitudes. Thus, the buoyancy frequencies can never be larger than the corresponding cut-off frequencies in either the isothermal case or the non-isothermal one. Nevertheless, this result does not exclude at some altitudes, when we compare the difference of the isothermal and nonisothermal cases, $\omega_a < \omega_B$ (say, 100-180 km) or $\omega_A < \omega_b$ (e.g., 70-80 km). This warns us to be cautious in applications about which thermal conditions are used, isothermal or non-isothermal? It is not accurate to use isothermal cutoff frequency and nonisothermal buoyancy frequency together, nor nonisothermal cutoff frequency and isothermal buoyancy frequency together. The two sets of frequencies under isothermal and nonisothermal conditions, respectively, should not be confused and mixing up, especially in wave analysis and data-fit modeling.

Compared with the vertical profiles of atmospheric properties, NRLMSISE-00 and HWM93 also provide the horizontal gradients of ρ_0, T_0, p_0, U, and V. These inhomogeneities are always at least $10^{2\sim3}$ smaller than the vertical gradients. It is reasonable to assume, as most authors did, that the mean-field parameters are uniform and stratified in the horizontal plane, free of any inhomogeneities compared to that in the vertical direction, i.e., $\partial/\partial x \simeq 0$, $\partial/\partial y \simeq 0$ and $\nabla \cong (\partial/\partial z)\hat{\mathbf{e}}_z$. Besides, we assume an intrinsic wave-frequency Ω and a horizontal wave-number k_h equivalent to a period of 30 minutes and a wavelength of ∼50 km, respectively, based on the data of the relations between horizontal wavelength and wave periods during the SpreadFEx campaign (*Taylor et al.* 2009).

Notes

Notes

b) Profiles of m_r and m_i in different models

To manifest the nonisothermal and wind-shear effects on the propagation of gravity waves, we compare the vertical profiles of growth rate m_i and vertical wavenumber m_r calculated from the three dispersion relations of (1) Eq.(1), which is from *Hines* (1960)'s classical isothermal and windless model; (2) Eqs.(8,10) of extended Hines's model in the presence of nonisothermality (namely, vertical temperature gradient) and wind shears (namely, vertical zonal and meridional wind gradients) as described in Section 2; and, (3) Eqs.(20,21) of the WKB approach as discussed in Section 3. The result is depicted in Fig.3. The LHS panel plots m_i and the RHS one symbolizes $\pm m_r$. In the panels, solid black lines, dotted red lines, and dash blue lines represent Hines', extended Hines', and WKB models, respectively.

The LHS panel let us be aware that above ∼200 km altitude the three growth rates converge to one profile. Below this height there appears the divergence. See the *Hines'* growth rate first of all. This is the classical result in gravity wave studies. According to Eq.(1), the rate is only determined by temperature T_0: $m_i = -1/(2H) = -g/(2R_sT_0)$. Thus, its vertical profile is correlated directly to the change of T_0 shown in the upper left panel of Fig.2. At the sea level, *Hines'* rate is -0.3 per 10 km. It reduces to -0.4 per 10 km at 13 km altitude, and then recovers to -0.3 per 10 km at 47 km. It falls down again to -0.6 per 10 km till 88 km, followed by an increase continuously in altitude to saturate at roughly -0.06 per 10 km above 200 km. Relative to *Hines'* model, the extended Hines' model is appreciably modulated, with a singularity at around 100±20 km altitude, where m_i soars up to $+\infty$ from below the altitude, and tends sharply down to $-\infty$ from above the altitude. This is caused by the zero phase speed $C_{ph} = 0$. Checking Eq.(8 leads us to confirm that the modulation comes from the wind-shear term, V_{k1}/C_{ph}. Below the 80 km altitude the shear modulation is much smaller. By contrast, above 120 km the growth rate fluctuates a complete cycle around *Hines'* profile. Concerning the WKB growth rate, although Eq.(20) includes both an additional nonisothermal term, k_T, and a coefficient, β, attached to the wind-shear term, its vertical profile keeps impressively away from the complicated extended Hines' model, but follows *Hines'* isothermal/shear-free model, except a little departure below 200 km altitude. We thus suggest that the extended Hines' model may exaggerate the shear effect due to the absence of the nonisothermal term in m_i; whileas the WKB model involves both nonisothermal and wind-shear effects and thus is able to provide a more realistic m_i-profile, which is surprisingly much closer to Hines' result after avoiding the nonisothermal deficiency in the extended Hines' model. This confirms *Hickey* (2011)'s argument that the WKB approach offers a more accurate picture for gravity waves propagating in realistic atmosphere by focusing on the vertical properties of perturbations.

In the RHS panel the three vertical wavenumbers (m_r) calculated from the three models reveal a more interesting result. As given in Eq.(1), *Hines'* model is only determined by the temperature profile T_0. By contrast, the extended Hines's model and the WKB one are dependent of not only T_0 but also its gradient (k_T) and wind shears (V_{k1}/C_{ph}), as given in both Eq.(10) and Eq.(21). The two profiles superimpose upon each other, and deviate from *Hines'*s model, though not significant. Similar to the LHS panel, there exists a discontinuity in the 80–120 km layer, contributed by $C_{ph} = 0$. Towards 300 km altitude

and beyond, the difference among the three models are increasingly disappearing with height. We notice that, although Eq.(10) and Eq.(21) are cogently discrepant due to the difference in shear-related terms (V_{k1}/C_{ph}):

$$\frac{1}{2}\left(\frac{2-\gamma}{\gamma H}-\frac{1}{2}\frac{V_{k1}}{C_{ph}}\right) \quad \text{versus} \quad \beta\left[\frac{2-\gamma}{\gamma H}-(3\beta-2)\,k_T-3(\beta-1)\frac{V_{k1}}{C_{ph}}+\frac{V_{k2}}{V_{k1}}\right] \tag{22}$$

there are α and β coefficients attached to ω_A and ω_B, respectively, in the WKB approach. The existence of these two coefficients make the complicated WKB expressions to produce an identical profile to that of the extended Hines' model. We thus suppose that, with a simpler mathematical expression but a complete recovery of the WKB result, the extended Hines' model is convenient and sufficient to account for the features of the vertical wavenumber in dealing with the propagation of gravity waves, particularly in ray-tracing mapping and its data-fit simulations.

c) Profiles of wave amplitudes in different models

Nonisothermality and wind-shears influence the vertical growth of gravity wave amplitudes. Fig.4 delineates the vertical profiles of atmospheric wave growth from (1) Hines' model (top left panel); (2) extended Hines' model (top right panel); and (3) the WKB approach (lower six panels) under initial conditions of $w_0 = 1.17\times10^{-4}$ m/s and $\mathrm{d}w_0/\mathrm{d}z = 0$ for wave-period $T = 33.3$ minutes. In the top two panels, the horizontal axis is the dimension-free amplitude growth, $A^* = A(z)/A(0)$, calculated from Eq.(11). The WKB results are produced by Eqs.(16,17).

The top LHS panel discloses the vertical profile of A^* calculated from *Hines'* model. First of all, the A^*-magnitude has an exact exponential growth in altitude, which reaches 7 at the 300 km altitude, reproducing *Hines* (1960)'s result. Secondly, the two envelops produced by $\exp(\int \mathrm{d}z/2H)$ and $\exp(z/2H_{400})$, respectively, are identical above 200 km altitude but with a little divergence (no more than 15%) in the 80-140 km layer, where $H_{400} = 67.1$ km is the scale height at the 400 km altitude. It is therefore reliable to use 67.1 km as the altitude-independent scale height under 300 km, particularly above 150 km altitude. Thirdly, between 200 km and 300 km, there are 6.5 cycles in the oscillation of the perturbed amplitude. This is consistent with the m_r-profile in Fig.4: above 200 km altitude $m_r \sim 0.4$ km^{-1}, corresponding to a wavelength of ~16 km in the vertical perturbation; this wavelength gives rise to 6.5 cycles within a 100 km layer. After including the effects of non-isothermality and windshears, the above features have discernable modifications, respectively, as exposed in the top RHS panel calculated from the extended *Hines'* model. At first, the exponential increase is now damped from 7 to 6 at the 300 km altitude due to the appearance of the damping factor $\kappa = 1 - HV_{k1}/C_{ph}$. In addition, the extended profile has a bulge which modifies the exponentially-growing envelop within the 100-150 km layer. From the U/V profiles in Fig.2 we suggest that this abnormality is related to the violent shears of the neutral wind. Finally, there are 7.5 cycles above the 200 km altitude, indicating that realistic atmosphere has a little shorter vertical wavelength, ~14 km, than *Hines'* idealized model due to the presence of the temperature & horizontal wind gradients. Note that based on Eq.(3) the amplitudes of all the six atmospheric

perturbations, i.e., p_1/p_0, ρ_1/ρ_0, T_1/T_0, u/U, v/V, and w, follow the same rule versus altitude in *Hines*' and extended *Hines*' models. It is seen that gravity waves propagate upward with an amplitude amplified exponentially or slightly damped, with an oscillation the frequency of which is determined by or a little modified from $m_r(z)$.

Notes

The lower six panels in Fig.4 demonstrate the perturbations of the six perturbed parameters under the WKB approach. The simulations use the adaptive-step, 4th-order Runge-Kutta method to calculate Eq.(16) under the initial conditions w_0 and $\mathrm{d}w_0/\mathrm{d}z$. At each step, after solving $w(z)$ and $\mathrm{d}w/\mathrm{d}z$, Eq.(17) is applied to obtain the perturbations of $p_1/p_0, \rho_1/\rho_0, T_1/T_0$ and u, v. Notice that the initial conditions of these 5 perturbations are all determined by w_0 and $\mathrm{d}w_0/\mathrm{d}z$. Firstly, all the perturbations have a same vertical wavelength. For example, above the 200 km altitude, there are 8.5 cycles, presenting a further shorter vertical wavelength, 12.5 km, than the previous *Hines*' model and the extended *Hines*' model. Secondly, unlike the identical profile of the amplitude growths for all the perturbations in *Hines*' two models, the WKB model gives different envelops of the atmospheric parameters to present distinct characteristics. For instance, the maximal amplitude of p_1/p_0 is smaller than that of both ρ_1/ρ_0 and T_1/T_0, while the phases of the last two are opposite. In addition, the perturbed components in velocity, u, v, w, evolve differently versus altitude. Take their amplitudes at the 300 km altitude as an example: their amplitudes are of 90 m/s, 550 m/s, and 140 m/s, respectively. In view of the vertically growing envelops, all the profiles have much smaller magnitudes than that of Hines' model, as shown in the middle right panel (in pink), above 100 km altitude, while below ∼80 km altitude all the perturbations appear to be zero. Notice that the three perturbations in pressure, density, and temperature satisfy the perturbed equation of state, $p_1/p_0 = \rho_1/\rho_0 + T_1/T_0$.

d) Inuence of phase speed in different models

The intrinsic phase speed, C_{ph}, affects the propagation of gravity waves in the three models introduced above. The relations are given by Eq.(1) in *Hines*' model, by Eqs.(8,10) in the extended *Hines*' model, and Eqs.(20,21) in the WKB approach. Fig.5 delineates the influence of dimension-free parameter, C_{ph}/C, on amplitude A^* in the two Hines' models (top panel), and on m_i (lower left) as well as m_r (lower right) of the three models at 100 km altitude where $C = 293$ m/s. Assume C_{ph}/C changes from 0 to 1.

In the top panel, *Hines*' A^* (in blue) flies up from 1 at $C_{ph}/C = 0$ to 2350 at $C_{ph}/C = 1$. By contrast, the extended *Hines*' A^* (in pink) experiences a sharp drop to nearly 0.1 within $C_{ph}/C < 0.1$ and then climbs up gradually to 33 at $C_{ph}/C = 1$. The ratio between the two values of A^* (in black) increases from 1 at $C_{ph}/C = 0$ and reaches to 72 at $C_{ph}/C = 1$. Review the top right panel of Fig.4. At the 106 km altitude, the ratio is 69, corresponding to $C_{ph} = 0.93C = 272$ m/s.

In the lower left panel, the dependence of m_i on C_{ph}/C has different features among the three models. In *Hines*' model (in blue), m_i keeps constant versus C_{ph}/C. In the extended *Hines*' model (in pink), m_i drops rapidly from infinity to about -0.7 $(10\mathrm{km})^{-1}$

with the increase of C_{ph}/C, and $m_i = 0$ at $C_{ph}/C = 0.074$. On the contrary, in the WKB case, m_i builds all the way up with C_{ph}/C from -0.58 $(10\text{km})^{-1}$ to infinity, with $m_i = 0$ at $C_{ph}/C = 0.791$. Similar to m_i, the dependence of m_r on C_{ph}/C in the lower right panel also exposes differences among the three models. *Hines'* case decreases continuously from infinity at $C_{ph}/C = 0$ to 0 at $C_{ph}/C = 0.9$. For the extended *Hines'* model and the WKB approach, both curves superimpose upon each other for $C_{ph}/C < 0.5$, falling down from infinity to $m_r = \pm 0.2$; they keep dropping but with different rates: the former reach zero at $C_{ph}/C = 0.97$ while the latter is at a smaller value of $C_{ph}/C = 0.75$. Beyond these two phase speeds, respectively, the former increases a little to ± 0.02 km^{-1}, while the latter rises rapidly to infinity.

V. Summary and Discussion

Gravity waves were extensively studied in the 1950s-1960s, when rudimentary theories and a myriad of effects were investigated (e.g., *Gossard & Munk* 1954; *Eckart* 1960; *Tolstoy* 1963; *Journal of Atmospheric and Terrestrial Physics* 1968; *Georges* 1968; and *AGARD* 1972). Since then, the understandings of the wave physics and its role played in the interactions between atmosphere and ionosphere have gained considerable progress (see details in, e.g., *Fritts & Alexander* 2003; *Fritts & Lund* 2011). The advance is dominantly achieved with a couple of approaches: (1) linear wave analysis under WKB-approximation (e.g., *Pitteway & Hines* 1963; *Einaudi & Hines* 1971; *Hines* 1971; *Gill* 1982; *Hickey & Cole* 1987,1988; *Nappo* 2002; *Vadas* 2007); (2) FWM formalism of vertical perturbation (e.g., *Lindzen & Tung* 1976; *Hickey et al.* 1997, 1998, 2000, 2001; *Liang et al.* 1998; *Walterscheid & Hickey* 2001; *Schubert et al.* 2003, 2005).

Realistic atmosphere is not isothermal and shear-free. It is featured by large temperature and wind-speed gradients especially in the vertical direction. Experiments demonstrated that the gradients can reach up to 100° K per km and 100 m/s per km, respectively (see, e.g., *Liu & Swenson* 2003; *She et al.* 2009). It is thus necessary to take into account these factors in theoretical modeling and data-fit studies. In this paper, we extended *Hines'* locally isothermal and shear-free model by including the nonisothermal and wind-shear effects, and derive dispersion relation of gravity waves by applying the WKB approximation. Exact analytical expressions of growth rate (m_i) and vertical wavenumber (m_r) are obtained. The nonisothermality is found to influence wave propagation through the vertical temperature gradient, as denoted by the temperature inhomogeneous number k_T, which extends the isothermal buoyancy and cut-off frequencies to their nonisothermal counterparts. In the WKB approach, k_T also contributes to a coefficient α. By contrast, the wind-shear exerts its impact through the combined effect of the vertical wind gradient (V_{k1}) and the intrinsic horizontal phase speed (C_{ph}).

We compare the extended *Hines'* model with the WKB results within 300 km altitude (note that the non-dissipation condition satisfies below 200 km altitude) with an arbitrary 50-km horizontal wavelength and 33.3-minute wave period. The vertical profiles of the background atmospheric properties and the horizontal winds are calculated from the empirical neutral atmospheric models NRLMSISE-00 and HWM93. Simulations expose

Notes

Notes

that the extended *Hines*' m_i-profile deviates away from *Hines*' model further than the WKB one due to the lack of the non-isothermal effect. In addition, the two m_r curves obtained from the extended *Hines*' and the WKB models superimpose upon each other, both of which amplify *Hines*' m_r magnitudes in the vertical direction. What is more, all the perturbations in the extended *Hines*' model has an identical profile in the growth of amplitude. This profile has a slight modification to the *Hines*' classical model except the 100-150 km layer. By contrast, the WKB model provides respective profiles of perturbations in pressure, density, temperature, zonal wind, meridional wind, and vertical wind. Finally, the propagation of gravity waves is related to the phase speed (C_{ph}): when it increases, the *Hines*' m_i-profile keeps constant, but the extended *Hines*' m_i drops down continuously while the WKB one soars up monotonously; at the same time, the three m_r profiles fall off together when C_{ph} is no more than $0.75C$, the two profiles obtained from the extended Hines' & the WKB models overlap upon each other which shift away from Hines' model.

VI. Acknowledgments

This work was done at the Embry-Riddle Aeronautical University (ERAU), Daytona Beach, FL. J. Ma thanks Professor M.P. Hickey, J.B. Snively, and M.D. Zettergren for the financial supports. Copies of the simulation runs and figures can be obtained by emailing to zma@mymail.ciis.edu.

References Références Referencias

1. AGARD (1972), Effects of atmospheric acoustic gravity waves on electromagnetic wave propagation, *Conf. Proc., 115*, Harford House, London.
2. Beer, T. (1974), Atmospheric Waves, John Wiley, New York.
3. Dutton, J. A. (1986), The Ceaseless Wind, Dover, New York.
4. Eckart, C. (1960), Hydrodynamics of oceans and atmospheres, Pergamon, New York.
5. Eckermann, S. D. (1997), Inuence of wave propagation on the Doppler spreading of atmospheric gravity waves, *J. Atmos. Sci., 54*, 2554-2573.
6. Einaudi, F., and C. O. Hines (1971), WKB approximation in application to acousticgravity waves, *Can. J. Phys., 48*, 14581471.
7. Francis, S. H. (1973), Acoustic-gravity modes and large-scale traveling ionospheric disturbances of a realistic, dissipative atmosphere, *J. Geophys. Res., 78*, 2278-2301.
8. Fritts, D. C., and M. J. Alexander (2003), Gravity wave dynamics and effects in the middle atmosphere, *Rev. Geophys., 41*, 1003, doi:10.1029/2001RG000106.
9. Fritts, D. C., and T. S. Lund (2011), Gravity wave inuences in the thermosphere and ionosphere: Observations and recent modeling, in: *Aeronomy of the Earths Atmosphere and Ionosphere*, ed.: Abdu, M. A., Pancheva, D., and Bhattacharyya, A., Springer, 109130.
10. Galperin, B., S. Sukoriansky, and P. S. Anderson (2007), On the critical Richardson number in stably stratified turbulence, *Atmos. Sci. Let., 8*, 6569.
11. Georges, T. M. (1968), Acoustic-gravity waves in the atmosphere, Symposium Proceedings, U.S. Government Printing Office, Washinton, D. C.
12. Gill, A. E. (1982), Atmosphere-ocean dynamics. Academic Press, Orlando, FL, International Geophysics Series.

13. Goldstein, S. (1931), On the instability of superposed streams of fluids of different densities, *Proc. R. Soc. London, Ser. A, 132*, 524-548.
14. Gossard, E. E., and W. H. Hooke (1975), Waves in the Atmosphere, Elsevier, New York.
15. Gossard, E. E., and W. H. Munk (1954), On gravity waves in the atmosphere, *J. Meteorol., 11*, 259-269.
16. Harris, I. and W. Priester (1962), Time dependent structure of the upper atmosphere, *J. Atmos. Sci., 19*, 286-301.
17. Hecht, J. H., R. L. Walterscheid, M. P. Hickey, and S. J. Franke (2001), Climatology and modeling of quasi-monochromatic atmospheric gravity waves observed over Urbana Illinois, *J. Geophys. Res., 106*, 51815196.
18. Hedin, A. E., E. L. Fleming, A. H. Manson, F. J. Schmidlin, S. K. Avery, R. R. Clark, S. J. Franke, G. J. Fraser, T. Tsuda, F. Vial, and R. A. Vincent (1996), Empirical wind model for the upper, middle and lower atmosphere, *J. Atmos. Terr. Phys.* 58, 1421-1447.
19. Hickey, M. P. (2001), Airglow variations associated with nonideal ducting of gravity waves in the lower thermosphere region, *J. Geophys. Res.*, 106, 17,90717,918.
20. Hickey, M. P. (2011), Atmospheric gravity waves and effects in the upper atmosphere associated with tsunamis, in: The Tsunami Threat – Research and Technology, ed.: Nils-Axel MArner, ISBN: 978-953-307-552-5, In Tech, Croatia and Shanghai.
21. Hickey M. P., and K. D. Cole (1987), A quantic dispersion equation for internal gravity waves in the thermosphere, *J. Atmos. Terr. Phys., 49*, 889-899.
22. Hickey M. P., and K. D. Cole (1988), A numerical model for gravity wave dissipation in the thermosphere, *J. Atmos. Terr. Phys.*, *50*, 689697.
23. Hickey, M. P., Richard L. Walterscheid, Michael J. Taylor, William Ward, Gerald Schubert, Qihou Zhou, Francisco Garcia, Michael C. Kelly, and G. G. Shepherd (1997), Numerical simulations of gravity waves imaged over Arecibo during the 10-day January 1993 campaign, *J. Geophys. Res., 102*, 11,475-11,489.
24. Hickey, M. P., M. J. Taylor, C. S. Gardner, and C. R. Gibbons (1998), Full-wave modeling of small-scale gravity waves using Airborne Lidar and Observations of the Hawaiian Airglow (ALOHA-93) O(^{1}S) images and coincident Na wind/temperature lidar mea- surements. *J. Geophys. Res.*, *103*, 6439-6453.
25. Hickey, M. P., R. L. Walterscheid, and G. Schubert (2000), Gravity wave heating and cooling in Jupiters thermosphere, *Icarus, 148*, 266–281.
26. Hickey, M. P., G. Schubert, and R. L. Walterscheid (2001), Acoustic wave heating of the thermosphere, *J. Geophys. Res., 106*, 2154321548.
27. Hickey, M. P., G. Schubert, and R. L. Walterscheid (2009), Propagation of tsunami-driven gravity waves into the thermosphere and ionosphere, *J. Geophys. Res., 114*, A08304, doi:10.1029/2009JA014105.
28. Hickey, M. P., G. Schubert, and R. L. Walterscheid (2010), Atmospheric airglow uctuations due to a tsunami-driven gravity wave disturbance, *J. Geophys. Res., 115*, A06308, doi:10.1029/2009JA014977.
29. Hines, C. O. (1960), Internal atmospheric gravity waves at ionospheric heights, *Can. J. Phys., 38*, 1441-1481.
30. Hines, C. O. (1971), Generalization of the Richardson criterion for the onset of atmospheric turbulence, *Q. J. R. Met Soc., 97*, 429-439.
31. Howard, L. (1961), Note on a paper of John W. Miles, *J. Fluid Mech., 10*, 509512.

Notes

32. Isler, J. R., M. J. Taylor, and D. C. Fritts (1997), Observational evidence of wave ducting and evanescence in the mesosphere, *J. Geophys. Res., 102*, 26,30126,313.
33. Journal of Atmospheric and Terrestrial Physics (1968), Symposium on upper atmospheric winds, waves and ionospheric drift, *J. Atmos. Terr. Phys.* (Spec. Issue), 30 (5).
34. Landau, L. D., and E. M. Lifshitz (1959), Fluid mechanics, Pergamon, New York.
35. Liang, J., W. Wan, and H. Yuan (1998), Ducting of acoustic-gravity waves in a nonisothermal atmosphere around a spherical globe, *J. Geophys. Res., 103*, 11,22911,234.
36. Lindzen, R. S., and K.-K. Tung (1976), Banded convective activity and ducted gravity waves, *Mon. Wea. Rev., 104*, 16021617.
37. Liu, H.-L. (2007), On the large wind shear and fast meridional transport above the mesopause, *Geophys. Res. Lett., 34*, L08815, doi:10.1029/2006GL028789.
38. Liu, A. Z., and G. R. Swenson (2003), A modeling study of O_2 and OH airglow perturbations induced by atmospheric gravity waves, *J. Geophys. Res., 108*, 4151, doi:10.1029/2002JD002474, D4.
39. Liu, X., J. Xu, J. Yue, and S. L. Vadas (2013), Numerical modeling study of the momentum deposition of small amplitude gravity waves in the thermosphere, *Ann. Geophys., 31*, 114.
40. Majda, A., and M. Shefter (1998), Elementary stratified ows with instability at large Richardson number, *J. Fluid Mech., 376*, 319350.
41. Marks, C. J., and S. D. Eckermann (1995), A three-dimensional nonhydrostatic raytracing model for gravity waves: Formulation and preliminary results for the middle atmosphere, *J. Atmos. Sci., 52*, 1959-1984.
42. Miles, J. (1961), On the stability of heterogeneous shear ows, *J. Fluid Mech., 10*, 496508.
43. Miles, J. (1986), Richardsons criterion for the stability of stratified shear ow, *Phys. Fluids, 29*, 3470.
44. Nappo, C. J. (2002), An Introduction to Atmospheric Gravity Waves, Academic, San Diego, California.
45. Picone, J. M., A. E. Hedin, D. P. Drob, and A. C. Aikin (2002), NRLMSISE-00 empirical model of the atmosphere: Statistical comparisons and scientific issues, *J. Geophys. Res.*, 107(A12), 1468, doi:10.1029/2002JA009430.
46. Pitteway, M. L. V., and C. O. Hines (1963), The viscous damping of atmospheric gravity waves, *Can. J. Phys., 41*, 19351948.
47. Pitteway, M. L. V., and C. O. Hines (1965), The reection and ducting of atmospheric acoustic-gravity waves, *Can. J. Phys., 43*, 22222243.
48. Schubert, G., M. P. Hickey, and R. L. Walterscheid (2003), Heating of Jupiters thermosphere by the dissipation of upward propagating acoustic waves, *ICARUS, 163*, 398-413.
49. Schubert, G., M. P. Hickey, and R. L. Walterscheid (2005), Physical processes in acoustic wave heating of the thermosphere, *J. Geophys. Res., 110*, DOI:10.1029/2004JD005488.
50. Snively, J. B., and V. P. Pasko (2003), Breaking of thunderstorm-generated gravity waves as a source of short-period ducted waves at mesopause altitudes, *Geophys. Res. Lett., 30*, 2254, doi:10.1029/2003GL018436.
51. She, C. Y., T. Li, B. P. Williams, T. Yuan, and R. H. Picard (2004), Concurrent OH imager and sodium temperature/wind lidar observation of a mesopause region

Notes

undular bore event over Fort Collins/Platteville, Colorado, *J. Geophys. Res., 109*, D22107, doi:10.1029/2004JD004742

52. She, C. Y., D. A. Krueger, R. Akmaev, H. Schmidt, E. Talaat, and S. Yee (2009), Longterm variability in mesopause region temperatures over Fort Collins, Colorado (41N, 105W) based on lidar observations from 1990 through 2007, *J. Terr. Sol. Atmos. Phys.*, 71, 15581564.
53. Snively, J. B., V. P. Pasko, M. J. Taylor, and W. K. Hocking (2007), Doppler ducting of short-period gravity waves by midlatitude tidal wind structure, *J. Geophys. Res., 112*, A03304, doi:10.1029/2006JA011895.
54. Sonmor, L. J., and G. P. Klaassen (1997), Toward a unified theory of gravity wave breaking, *J. Atmos. Sci., 54*, 26552680.
55. Stone, P. H. (1966), On non-geostrophic baroclinic stability, *J. Atmos. Sci., 23*, 390-400.
56. Sutherland, B. R. (2010), Internal gravity waves, Cambridge University Press, Cambridge.
57. Taylor, G. I. (1931), Effect of variation in density on the stability of superposed streams of fluid, *Proc. R. Soc. London, Ser. A, 132*, 499-523.
58. Taylor, M. J., D. N. Turnbull, and R. P. Lowe (1995), Spectrometric and imaging measurements of a spectacular gravity wave event observed during the ALOHA-93 campaign, *Geophys. Res. Lett., 22*, 28492852.
59. Taylor, M. J., P.-D. Pautet, A. F. Medeiros, R. Buriti, J. Fechine, D. C. Fritts, S. L. Vadas, H. Takahashi, and F. T. Sao Sabbas (2009), Characteristics of mesospheric gravity waves near the magnetic equator, Brazil, during the SpreadFEx campaign, *Ann. Geophys., 27*, 461472.
60. Tolstoy, I. (1963), The theory of waves in stratified uids including the effects of gravity and rotation, *Rev. Mod. Phys., 35*, 207-230.
61. Vadas, S. L. (2007), Horizontal and vertical propagation and dissipation of gravity waves in the thermosphere from lower atmospheric and thermospheric sources, *J. Geophys. Res., 112*, A06305, doi:10.1029/2006JA011845.
62. Vadas, S. L., and D. C. Fritts (2004), Thermospheric responses to gravity waves arising from mesoscale convective complexes, *J. Atmos. Sol. Terr. Phys., 66*, 781-804.
63. Vadas, S. L., and D. C. Fritts (2005), Thermospheric responses to gravity waves: Inuences of increasing viscosity and thermal diffusivity, *J. Geophys. Res., 110*, D15103, doi:10.1029/2004JD005574.
64. Volland, H. (1969a), Full wave calculations of gravity wave propagation through the thermosphere, *J. Geophys. Res., 74*, 17861795.
65. Volland, H. (1969b), The upper atmosphere as a multiple refractive medium for neutral air motions, *J. Atmos. Terr. Phys., 31*, 491-514.
66. Walterscheid, R. L., J. H. Hecht, R. A. Vincent, I. M. Reid, J. Woithe, and M. P. Hickey (1999), Analysis and interpretation of airglow and radar observations of quasimonochromatic gravity waves in the upper mesosphere and lower thermosphere over Adelaide, Australia (35S, 138E), *J. Atmos. Sol. Terr. Phys., 61*, 461478.
67. Walterscheid, R. L., and M. P. Hickey (2001), One-gas models with height-dependent mean molecular weight: Effects on gravity wave propagation, *J. Geophys. Res., 106*, 28,831-28,839.
68. Walterscheid, R. L., and M. P. Hickey (2005), Acoustic waves generated by gusty ow over hilly terrain, *J. Geophys. Res., 110*, DOI: 10.1029/2005JA011166.

Notes

69. Walterscheid, R. L., and M. P. Hickey (2012), Gravity wave propagation in a diffusively separated gas: Effects on the total gas, *J. Geophys. Res., 117*, A05303, doi:10.1029/2011JA017451.
70. Walterscheid, R. L., G. Schubert, and D. G. Brinkman (2001), Small-scale gravity waves in the upper mesosphere and lower thermosphere generated by deep tropical convection, *J. Geophys. Res., 106*, 31,82531,832.
71. Wang, D. Y., and T. F. Tuan (1988), Brunt-Doppler ducting of small period gravity waves, *J. Geophys. Res., 93*, 9916-9926.
72. Yu, Y., and M. P. Hickey (2007a), Time-resolved ducting of atmospheric acousticgravity waves by analysis of the vertical energy ux, *Geophys. Res. Lett., 34*, L02821, doi:10.1029/2006GL028299.
73. Yu, Y., and M. P. Hickey (2007b), Numerical modeling of a gravity wave packet ducted by the thermal structure of the atmosphere, *J. Geophys. Res., 12*, A06308, doi:10.1029/2006JA012092.
74. Yu, Y., and M. P. Hickey (2007c), Simulated ducting of high-frequency atmospheric gravity waves in the presence of background winds, *Geophys. Res. Lett., 34*, L11103, doi:10.1029/2007GL029591.
75. Zhou, Q. and Y. T. Morton (2007), Gravity wave propagation in a nonisothermal atmosphere with height varying background wind, *Geophys. Res. Lett., 34*, L23803, doi:10.1029/2007GL031061.

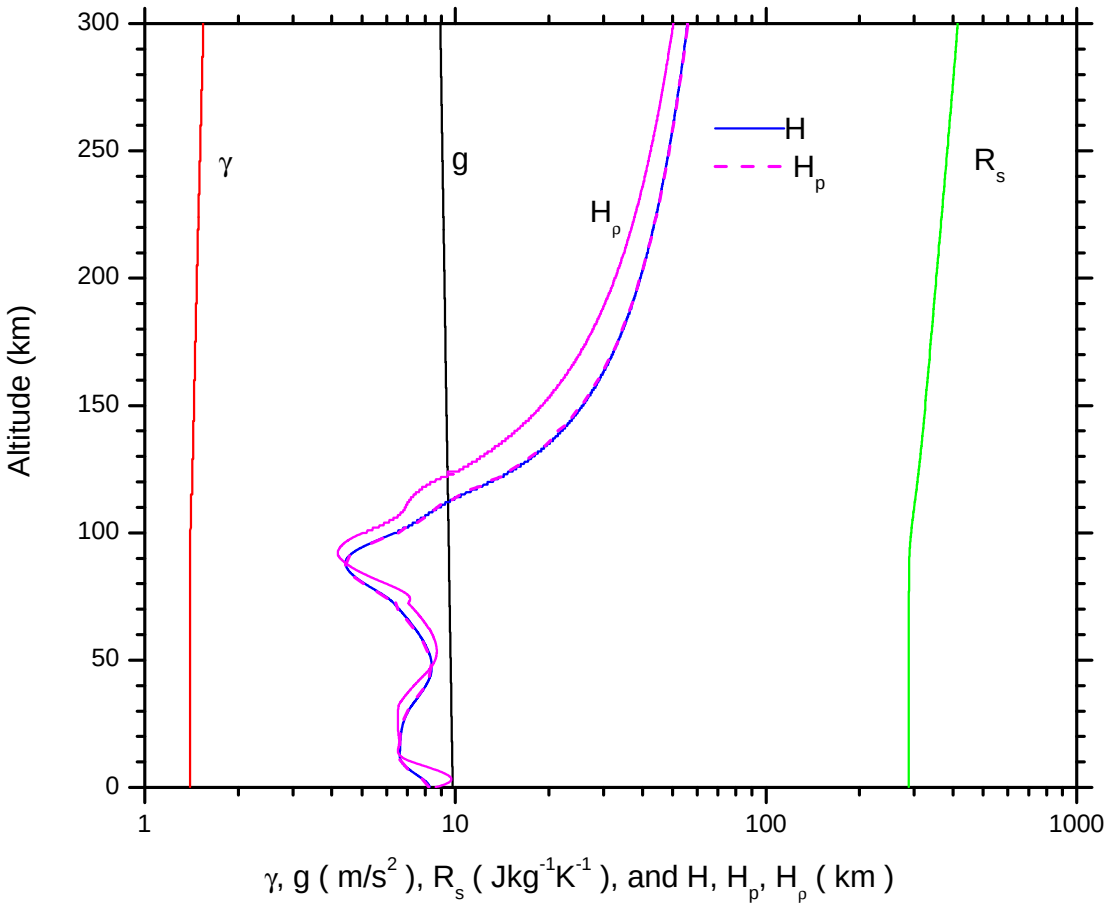

Figure 1 : Vertical pro˙les of input parameters in atmosphere: adiabatic index, γ (in red); gravitational acceleration, g (in black); specific gas constant, R_s (in green); and Hines' scale height, H (in blue), as well as the two scale heights in density, H_ρ (in solid pink), and in pressure, H_p (in dash pink), respectively. Note that $H = H_p \neq H_\rho$.

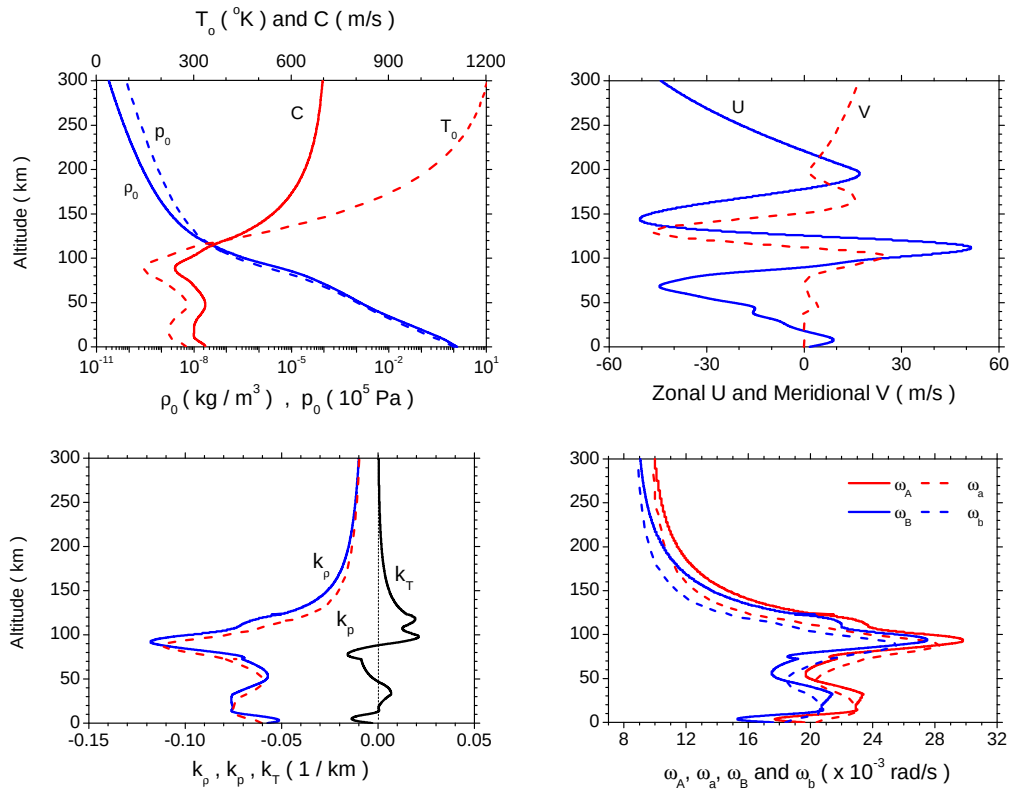

Figure 2 : Vertical profiles of atmospheric mean-field properties (upper two panels) from NRLMSISE-00 (*Picone et al.* 2002) and HWM93 (*Hedin et al.* 1996), and related gravity wave parameters (lower two panels). Upper left: mass density ρ_0 (solid blue), pressure p_0 (dash blue), sound speed C (solid red), and temperatur T_0 (dash red); upper right: zonal (eastward) wind U (solid blue) and meridional (northward) wind V (dash pink); lower left: density scale number k_ρ (solid blue), pressure scale number k_p (dash red), and temperature scale number k_T (solid black); lower right: cut-off frequencies ω_A (solid red) and ω_a (dash red), and buoyancy frequencies ω_B (solid blue) and ω_b (dash blue).

Notes

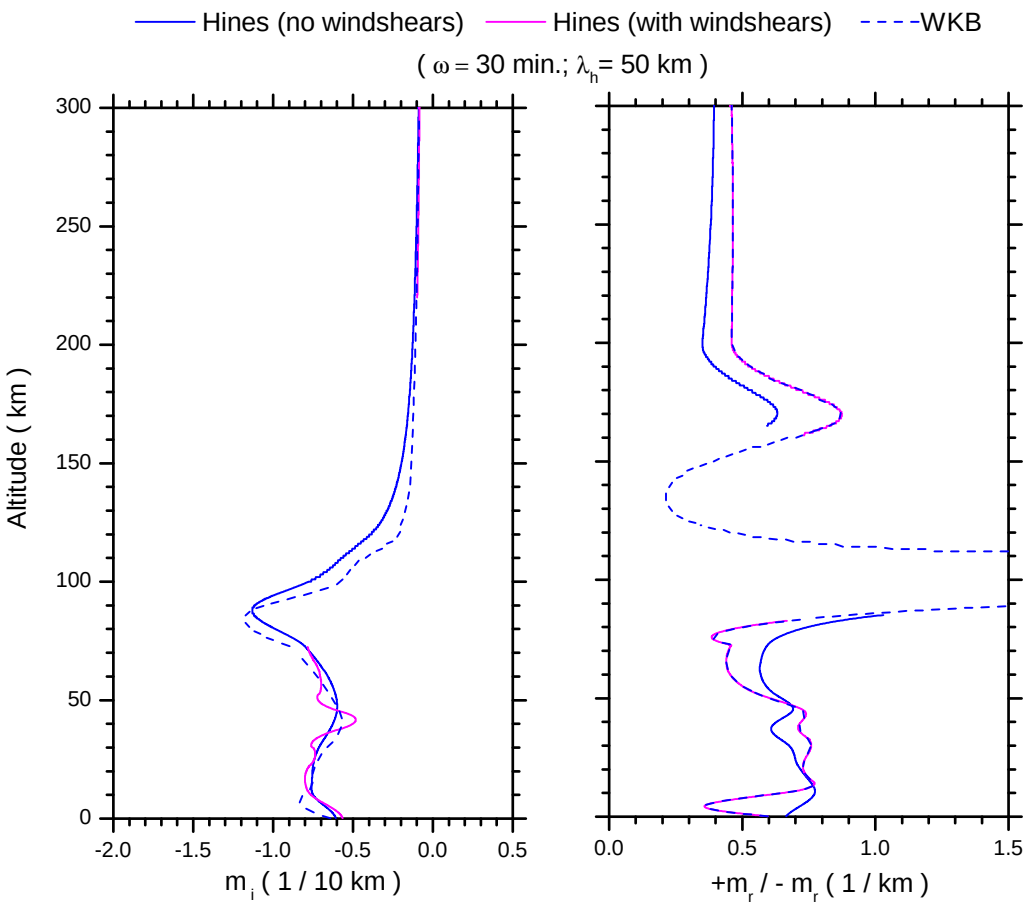

Figure 3 : Comparisons of growth rate m_i and vertical wavenumber m_r of gravity waves among three different dispersion relations: (1) *Hines* (1960)' non-windshear model (in solid blue), (2) Wind-shear model (Section 2; in red); and, (3) WKB model (Section 3; in dashed blue)

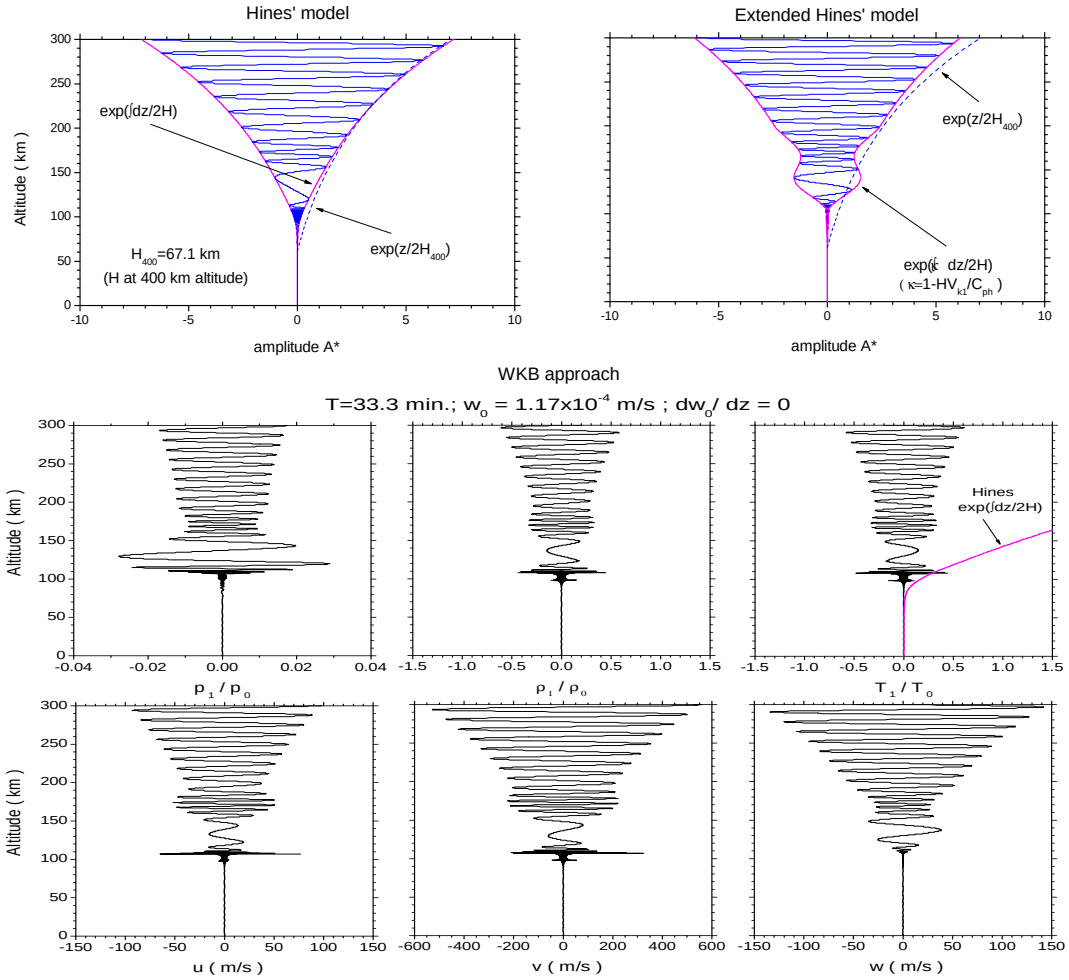

Figure 4 : Vertical growth of atmospheric perturbations from (1) Hines' model (top left panel); (2) extended Hines' model (top right panel); and (3) the WKB approach (lower six panels) under initial conditions of $w_0 = 1.17 \times 10^{-4}$ m/s and $\mathrm{d}w_0/\mathrm{d}z = 0$ for wave-period of $T = 33{:}3$ minutes. In the top two panels, $A^* = A(z)/A(0)$.

Notes

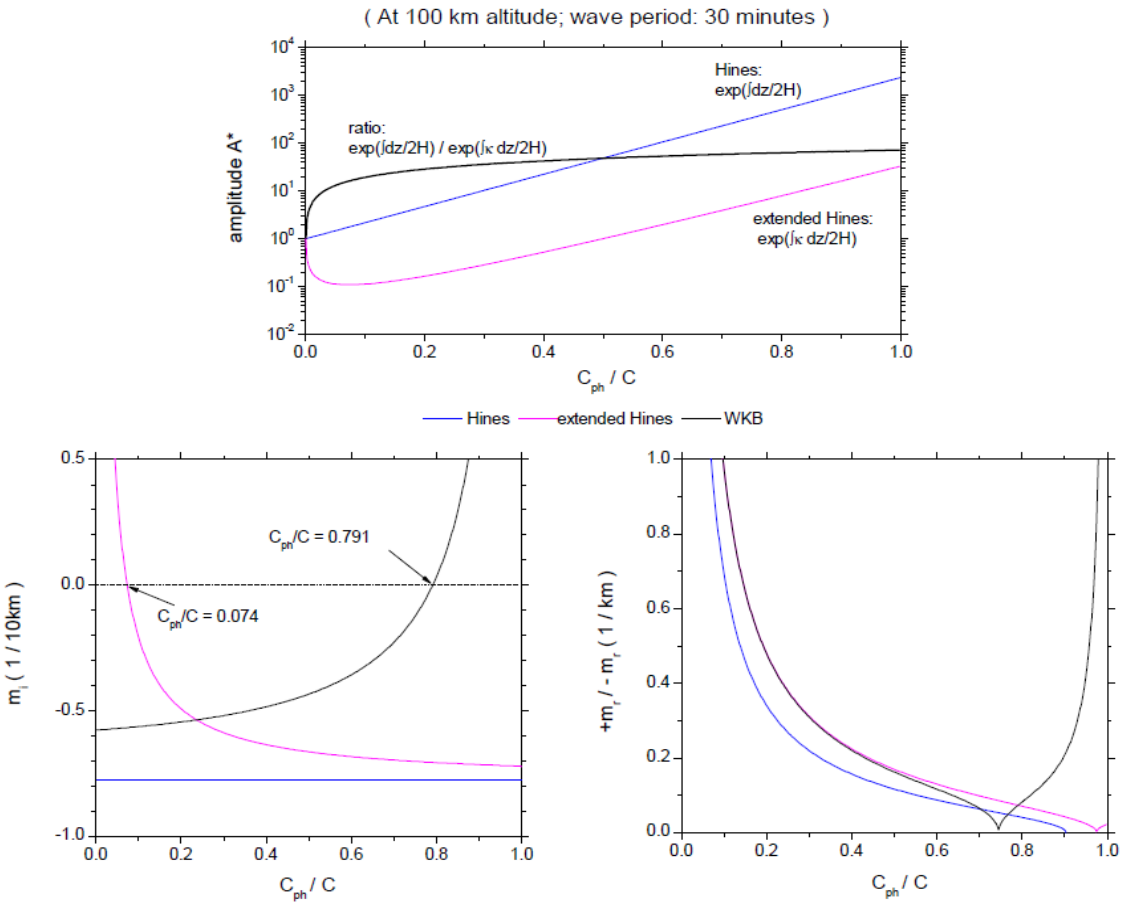

Figure 5 : Inuence of phase speed on the propagation of gravity waves in the three models